Phyton-
International Journal of
Experimental Botany

Tech Science Press

http://doi.org/10.32604/phyton.2025.073817

ARTICLE

PpCSC1, a Novel ERD4 Ortholog from *Physcomitrium patens*, Plays a Negative Role in Salt Stress Tolerance

Lu Chen[1,2,#], Zhijie Ren[2,#], Guangmin Zhao[2], Xuan He[2], Legong Li[2], Sheng Teng[1,*], Yikun He[2,*] and Fang Bao[2,*]

[1]Key Laboratory of Microbiological Metrology, Measurement & Bio-product Quality Security, State Administration for Market Regulation, College of Life Sciences, China Jiliang University, 258 Xueyuan Street, Hangzhou, 310018, China
[2]College of Life Sciences, Capital Normal University, 105 West Third Ring North Road, Beijing, 100048, China
*Corresponding Authors: Sheng Teng. Email: steng@cjlu.edu.cn; Yikun He. Email: yhe@cnu.edu.cn; Fang Bao. Email: 5838@cnu.edu.cn
#These authors contributed equally to this work

Received: 26 September 2025; Accepted: 15 December 2025; Published: 30 January 2026

ABSTRACT: ERD4 proteins, members of the early responsive-to-dehydration family, act as plasma membrane ion channels that contribute to ion homeostasis and modulate plant response to abiotic stresses. However, the functions of ERD4 homologs in non-vascular species remain largely unexplored. Here, we characterized an ERD4 family homolog in *Physcomitrium patens* (Hedw.) Mitt., PpCSC1 (Calcium-permeable Stress-responsive Cation Channel 1), and investigated its role in salt stress response. PpCSC1 localized to the plasma membrane and functioned as a non-selective cation channel permeable to Na^+, K^+, Ca^{2+}, and Mg^{2+}. Under salt treatment, *PpCSC1* transcripts were markedly downregulated, whereas overexpression lines exhibited enhanced salt sensitivity. Ion content analysis further revealed reduced K^+ accumulation, lowered K^+/Na^+ ratios, and elevated Mg^{2+} levels, collectively disrupting ionic homeostasis and impairing salt tolerance. Transcriptional regulation analysis revealed that the C2H2-type zinc finger transcription factor PpSTOP2 directly activated *PpCSC1* expression. Notably, *PpSTOP2* knockout plants displayed reduced *PpCSC1* mRNA accumulation and improved salt tolerance. Together, these findings indicate that PpCSC1 is a plasma membrane-localized cation channel that negatively regulates salt tolerance by disturbing ion balance, and that its regulation by PpSTOP2 integrates upstream signaling with downstream physiological responses. This work provides new insight into how non-selective ion channels shape stress adaptation in early land plants.

KEYWORDS: *Physcomitrium patens*; Calcium-permeable Stress-responxive Cation Channel 1 (PpCSC1); cation transport activity; salt stress; transcriptional regulation

1 Introduction

Plants are constantly exposed to various abiotic stresses, including drought, high salinity, osmotic fluctuations, and low temperature, which disrupt cellular ion balance and metabolic homeostasis, impair photosynthesis and growth, and can ultimately result in plant death [1–4]. To address these challenges, plants have developed sophisticated membrane-associated perception and signaling systems that rapidly activate stress-response pathways [5–9]. Among these, ion channels that directly sense osmotic changes and initiate downstream signaling events play a central role in the early stages of abiotic stress responses [10–13].

In *Arabidopsis thaliana* (L.) Heynh, 16 dehydration-responsive genes were originally identified and designated as early-responsive to dehydration (ERD) genes [14,15]. Among them, *ERD4* encodes a multi-pass

transmembrane protein that contains the highly conserved DUF221 domain (Pfam accession: 02714), a motif commonly found in stress-related ion channels [16–19]. ERD4 proteins, such as OSCA1 (Reduced Hyperosmolality-Induced $[Ca^{2+}]_i$ Increase 1) and AtCSC1 (Calcium-permeable Stress-responsive Cation Channel 1), function as osmosensitive ion channels that mediate rapid Ca^{2+} influx under hyperosmotic stress [16,17]. However, AtCSC1 conducts not only Ca^{2+}, but also other cations, including Na^+ and K^+ [17]. Structural studies on OSCA channels have demonstrated that they form lipid-gated homodimeric pores and share features with mechanosensitive ion channels [20–23]. Functionally, the rapid activation of OSCA1 under osmotic stress triggers Ca^{2+} signaling waves that regulate stomatal closure, root architecture adjustment, and transcriptional reprogramming [16].

In angiosperms, ERD4 homologs have been implicated in enhancing abiotic stress tolerance. For example, ZmERD4 in *Zea mays* L. is constitutively expressed in various tissues and is strongly induced by drought, salinity, and ABA treatment, but not by cold stress. Heterologous overexpression of *ZmERD4* in *A. thaliana* enhances tolerance to drought and salt [24]. Similarly, *BjERD4* from *Brassica juncea* (L.) Czern. is stress-inducible and exhibits RNA-binding activity, suggesting a potential role in post-transcriptional regulation during stress responses [18].

Despite these advances, the functions of ERD4 homologs in non-vascular plants remain largely unknown. *Physcomitrium patens* (Hedw.) Mitt., a model bryophyte, exhibits physiological traits of early land plants and demonstrates remarkable tolerance to drought, salinity, osmotic, and cold stress [25–28]. In response to salinity, *P. patens* activates a coordinated defense program that includes ion transporters such as PpENA1, PpSOS1, PpNHAD1, and PpHAK1/2, which help maintain K^+/Na^+ homeostasis [29–33], along with ROS-scavenging enzymes like PpAKR1A, which enhance antioxidative capacity [34,35]. Additionally, several regulators, including PpCIPK1, PpAOX, PpCKX1, AP2/ERF transcription factors, PpLEA3, and PpSARK, enhance salt adaptation in *P. patens* by promoting ion homeostasis, stabilizing mitochondrial redox balance, improving developmental and dehydration tolerance, controlling chloroplast division, enhancing osmotic and oxidative protection, and activating ABA-dependent signaling [36–41]. Together, these findings suggest that *P. patens* possesses a highly integrated network of ionic, redox, and transcriptional regulation for abiotic stress adaptation, highlighting its value as a model for understanding ERD4 function and the evolutionary origins of salt-stress tolerance in early land plants.

In parallel with membrane-mediated signaling, transcriptional regulators also play central roles in plant stress responses. Among them, STOP1 (Sensitive to Proton Rhizotoxicity 1), a C2H2-type zinc finger transcription factor in *A. thaliana*, is essential for tolerance to multiple abiotic stresses, particularly aluminum toxicity and low-pH conditions in acid soils [42–44]. STOP1 directly activates key transporter genes, such as *ALMT1*, *MATE*, and *ALS3*, which mediate organic acid efflux and facilitate detoxification [45–48]. STOP1-like proteins in *Oryza sativa* L. and other species perform similar functions in regulating responses to aluminum toxicity and low pH [49–53]. These findings highlight how plants integrate transcriptional regulation and membrane-based mechanisms to maintain ion homeostasis under stress conditions.

Here, we identified and characterized a novel ERD4 homolog from *P. patens*, designated *PpCSC1*. The encoded protein localizes to the plasma membrane and functions as a non-selective cation channel. Functional analyses revealed that overexpression of *PpCSC1* disrupts ion balance, lowers the K^+/Na^+ ratio, and reduces salt tolerance, suggesting a negative regulatory role in salt stress adaptation. Moreover, we identified the transcription factor PpSTOP2 as an upstream activator of PpCSC1. Loss of PpSTOP2 suppressed *PpCSC1* expression and enhanced salt tolerance under salt stress. Together, our findings reveal a regulatory module in which *PpCSC1*, controlled by PpSTOP2, acts as a negative regulator of salt tolerance in

moss. This study expands the functional understanding of ERD4 proteins in basal land plants and provides new insights into membrane-mediated sensing and signaling mechanisms during abiotic stress.

2 Materials and Methods

2.1 Plant Materials and Stress Treatments

Physcomitrium patens (Hedwig) ecotype 'Gransden 2004' was used as the wild-type strain. Protonema tissues were propagated axenically on solid BCD medium supplemented with 0.5% (*w*/*v*) glucose and 1 mmol L^{-1} $CaCl_2$, under a 16 h light/8 h dark cycle at 25°C with a light intensity of 50 μmol m^{-2} s^{-1} [54–56]. For analyzing the transcript levels of *PpCSC1* and *PpSTOP2* under salt stress, five-day-old protonemata were transferred to BCD medium containing 350 mmol L^{-1} NaCl and harvested at 0, 2, 4, 8, 12, or 24 h. Based on existing literature [28,36,57] and our preliminary results, five-day-old protonemata were grown on BCD medium containing 350 mmol L^{-1} or 500 mmol L^{-1} NaCl for 4 days to assess growth performance. The two concentrations were selected to provide gene-specific insights: 350 mmol L^{-1} NaCl allows visualization of the growth phenotype in *PpCSC1*-overexpressing lines, whereas 500 mmol L^{-1} NaCl is suitable for evaluating the function of PpSTOP2 under more severe salt stress. This experimental design enables a focused investigation of the distinct contributions of these genes to salt stress adaptation.

2.2 Quantitative Real-Time Reverse Transcription PCR (qRT-PCR) Analysis

Total RNA was isolated from plant tissues using the RNeasy Plant Mini Kit (Qiagen, Valencia, CA, USA), and contaminating genomic DNA was removed by gDNA Eraser (Takara Bio, Dalian, China). First-strand cDNA was synthesized using the PrimeScript RT reagent kit (Takara, China). The *P. patens* tubulin gene was used as the internal reference (forward primer: GAGTTCACGGAAGCGGAGAG; reverse primer: TCCTCCAGATCCTCCTCATA). Transcript levels were quantified using the SYBR® Premix Ex Taq™ Kit (Takara Bio, Dalian, China) on an ABI 7500 thermocycler (Applied Biosystems). The primers used for qRT-PCR were as follows: *PpCSC1* forward CGGACCTACAGGATTCGCTAA and reverse ATCTCCAGCACTGCAACGAAG; *PpSTOP2* forward GCCAATGTACAGAAGCAAGCCTA and reverse ATTCATCATCTGACTACTGAGCT. Relative expression values were calculated using the $2^{-\Delta\Delta Ct}$ method [58,59], with three independent biological replicates.

2.3 Plasmid Construction

For CRISPR/Cas9 mutagenesis of *PpSTOP2*, a 20-bp guide RNA (crRNA: TTGAGGGCAATGCTGTAGCC) targeting the first exon was designed using the CRISPOR V1 web tool based on the *P. patens* genome Phytozome V9 (http://crispor.tefor.net/crispor.py) [60]. The sgRNA, driven by the *P. patens* U3/U6 promoter, was fused with the *Streptococcus pyogenes* tracrRNA scaffold (Fabien Nogué) and cloned into the pUC57 backbone. The sgRNA plasmid, along with a Cas9 expression construct (*Sp-hCas9*) and pBNRF (Fabien Nogué), was introduced into *P. patens* protoplasts via PEG-mediated transformation.

The full-length coding sequence of *PpCSC1* was amplified from wild-type cDNA (primers: forward ATGACGGCAACTGGGGCTT; reverse GAGAGCATGGAACTCCTCTGTGC) and inserted downstream of the rice *Actin2* promoter in the binary vector pTFH15.3 to create an overexpression construct. For promoter activity assays, a 2.0-kb upstream fragment of *PpCSC1* was cloned into pTFH15.3-GUS vector using *SpeI*/*AscI* restriction sites to generate the *PpCSC1pro::GUS* construct.

2.4 Transformation of P. patens

Protoplast transformation was carried out following established PEG-mediated protocols [35]. Regenerated protoplasts were initially cultivated on BCD medium for 7 days and then transferred to selection plates containing G418 (25 mg L^{-1} for overexpression and fusion GUS transgenic lines; 50 mg L^{-1} for CRISPR/Cas9-based editing). Resistant colonies were subcultured on non-selective medium for recovery. The integration of exogenous DNA into the genomic DNA of stable transformants was verified by genomic PCR following the manufacturer's protocols, while CRISPR-induced mutations were confirmed by sequencing of the target locus.

2.5 Histochemical Analysis of GUS Activity

Transgenic lines carrying *PpCSC1pro::GUS* were stained for β-glucuronidase activity using a commercial staining buffer (Sbjbio, Nanjing, China). Protonemata (5 days) and gametophores (21 days) were incubated at 37°C for 10–12 h, washed in water for 10–60 min, and cleared in 70% ethanol. Staining was examined using Zeiss Axio Imager M2 (protonema) and Axio Zoom V16 (gametophore) microscopes [46]. Data were obtained from at least three independent lines showing consistent patterns.

2.6 Transient Transformation of A. thaliana Protoplasts

Transient expression in *A. thaliana* mesophyll protoplasts was carried out as described [61]. Reporter plasmids (*PpCSC1-LUC* and *Ubi-GU*) were co-transformed with effector plasmids using PEG-mediated transformation. After 12 h of incubation, protoplasts were lysed and clarified by centrifugation at 20,000× *g*. Luciferase activity was normalized to GUS activity (relative LUC = LUC/GUS). Data represent four biological replicates.

For subcellular localization, *PpCSC1-EGFP* was introduced into protoplasts and fluorescence was observed after 12 h using a Zeiss LSM 780 confocal microscope (Stuttgart, Germany). Two independent experiments showed consistent GFP localization patterns.

2.7 Determination of Total Chlorophyll Content

Fresh tissues were homogenized in 10 mL of extraction buffer (acetone: ethanol: Milli-Q water = 4.5:4.5:1). Absorbance at 645 nm and 663 nm was measured using a UV-Vis spectrophotometer. Chlorophyll concentrations were estimated using previously described equations [35].

2.8 Cation Content Determination

Five-day-old protonemal cultures of *P. patens* were transferred to BCD medium supplemented with 350 mmol L^{-1} NaCl for three days. The material was rinsed thoroughly with deionized water, then dried to constant mass at 98°C for 2–3 days. The dried samples were ground into a fine powder using mortar and pestle. Approximately 100 mg samples were digested with concentrated nitric acid, and ion concentrations were quantified by ICP-MS (Capital Normal University, Beijing, China).

2.9 Voltage-Clamp Experiment

The full-length coding sequence of *PpCSC1* was inserted into the pGEMHE expression plasmid for functional assays. Linearized plasmids (1 μg each) were used as templates for *in vitro* transcription with the mMESSAGE mMACHINE T7 kit (Ambion, Thermo Fisher Scientific, Austin, TX, USA), following the supplier's standard protocol to produce capped cRNAs. Defolliculated *Xenopus laevis* oocytes, after removal

of follicle cells, were microinjected with approximately 23 ng of cRNA per cell and then maintained in ND96 buffer at 18°C for four days before current recordings. Electrophysiological measurements were performed using the two-electrode voltage-clamp (TEVC) technique with a TEV-200 amplifier (Dagan Corp., Minneapolis, MN, USA). Data acquisition was performed using a Digidata 1440A interface coupled with pCLAMP 10.2 software (Molecular Devices/Axon Instruments, Foster City, CA, USA), with cells held at −60 mV. During recording, *Xenopus laevis* oocytes were continuously bathed in ND96 buffer containing 96 mmol L^{-1} NaCl, 2 mmol L^{-1} KCl, 1 mmol L^{-1} $MgCl_2$, 1.8 mmol L^{-1} $CaCl_2$, and 10 mmol L^{-1} HEPES, adjusted to pH 7.5 with NaOH, at ambient temperature. To test cation selectivity, NaCl in the external solution was equimolarly substituted with either KCl, $CaCl_2$ or $MgCl_2$.

3 Results

3.1 Phylogenetic Analysis of PpCSC1 within the Bryophyte ERD4 Family

Similar to *A. thaliana* AtCSC1 and OSCA1 [16,17,20], the moss ERD4 homolog *PpCSC1* encodes a protein of 749 amino acids. TMHMM-2.0 prediction (https://services.healthtech.dtu.dk/service.php?TMHMM-2.0) indicated that PpCSC1 contains ten transmembrane domains (Fig. 1a), with domains 4–10 forming the conserved DUF221 domain. Phylogenetic analysis revealed that moss ERD4 homologs form a distinct evolutionary clade, with PpCSC1 showing high sequence similarity to *A. thaliana* OSCA family member OSCA3.1 (Fig. 1b).

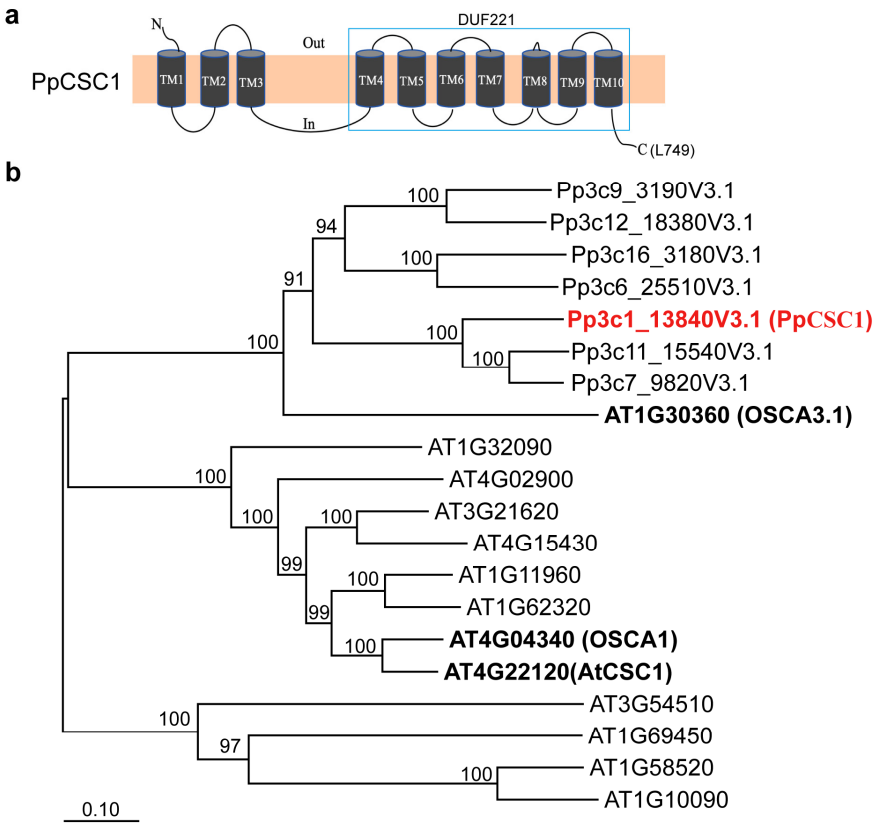

Figure 1: Phylogenic analysis of *PpCSC1* and its orthologous in bryophytes. (**a**) The predicted membrane topology and protein structure of PpCSC1. Transmembrane domains (TM) and the predicted pore-forming region are indicated. (**b**) Phylogenetic tree of ERD4 orthologs from *P. patens* and *A. thaliana*. Bootstrap support values (1000 replicates) are shown next to branches, and the scale bar represents the number of substitutions per site.

3.2 The PpCSC1 Protein Localizes in the Plasma Membrane

Subcellular localization was examined using a transient expression system in *A. thaliana* protoplast. The PpCSC1–GFP fusion protein exhibited a strong GFP signal at the plasma membrane (Fig. 2a).

Expression pattern was further assessed using *ProPpCSC1::GUS* reporter plants. GUS staining indicated predominant expression in protonemal tissues and in the central region of gametophyte leaves (Fig. 2b).

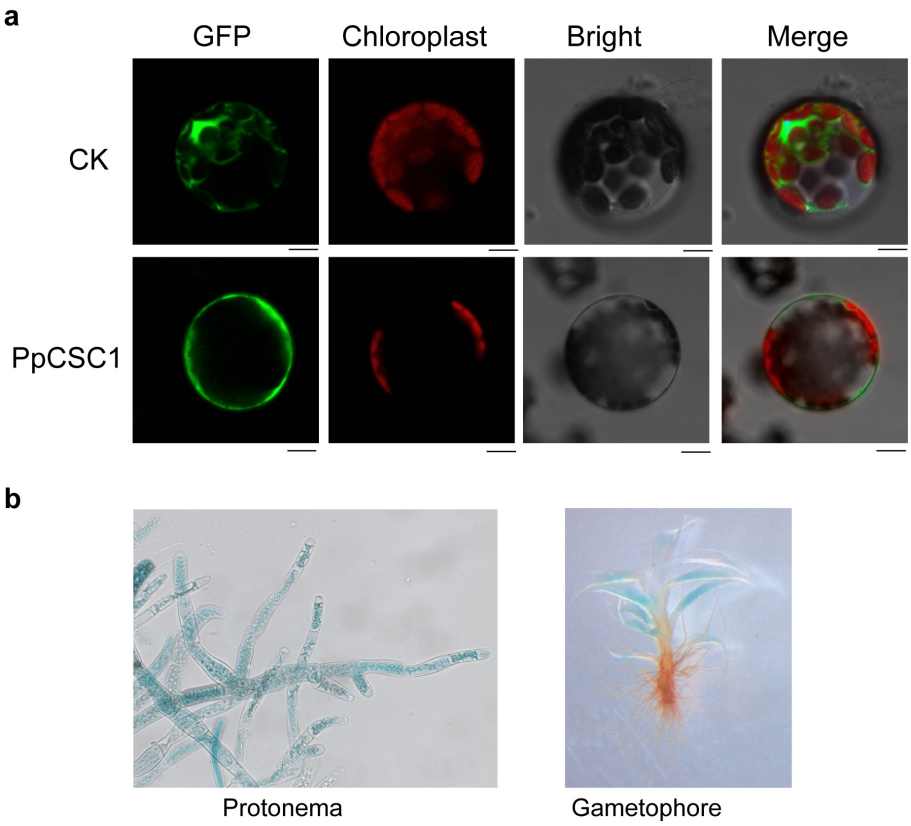

Figure 2: The subcellular localization and tissue specificity of PpCSC1 protein. (**a**) Subcellular localization of PpCSC1–GFP in *A. thaliana* protoplasts. From left to right: GFP fluorescence (green), chloroplast autofluorescence (red), bright-field (BF), and the merged image combining GFP, chloroplast, and BF signals. Images represent single confocal optical sections. Scale bar = 10 μm. (**b**) Tissue-specific expression patterns of *PpCSC1::GUS* in protonema (left) and gametophyte (right).

3.3 PpCSC1 Exhibits Cation Transport Activity

Since ERD4 family members in *A. thaliana* have been reported to function as osmosensitive cation channels [16,17,20,21], we investigated whether PpCSC1 exhibits similar activity using two-electrode voltage-clamp (TEVC) recording in the *Xenopus laevis* oocytes heterologous expression system. We replaced ND96 solution with 20 mmol L^{-1} NaCl, KCl, $CaCl_2$, or $MgCl_2$. Robust inward currents were detected in all conditions (Fig. 3a,b), demonstrating that PpCSC1 conducts multiple cations and functions as a non-selective cation channel.

We next investigated whether extracellular Ca^{2+} influences PpCSC1 activity. Perfusion with increasing Ca^{2+} concentrations (1, 5, and 10 mmol L^{-1}) enhanced current amplitudes in a dose-dependent manner, accompanied by shifts in reversal potentials (Fig. 3c,d), indicating Ca^{2+}-dependent regulation. Notably,

prominent tail currents were observed in Ca^{2+}-containing buffers, and these were attenuated by the Cl^- channel blocker DIDS (0.1 mM) (Fig. 3e), consistent with activation of endogenous Ca^{2+}-activated chloride channels (CACC). Furthermore, treatment with the Ca^{2+} channel inhibitor $GaCl_3$ strongly suppressed PpCSC1-mediated currents (Fig. 3f), confirming that its channel activity depends on external Ca^{2+}.

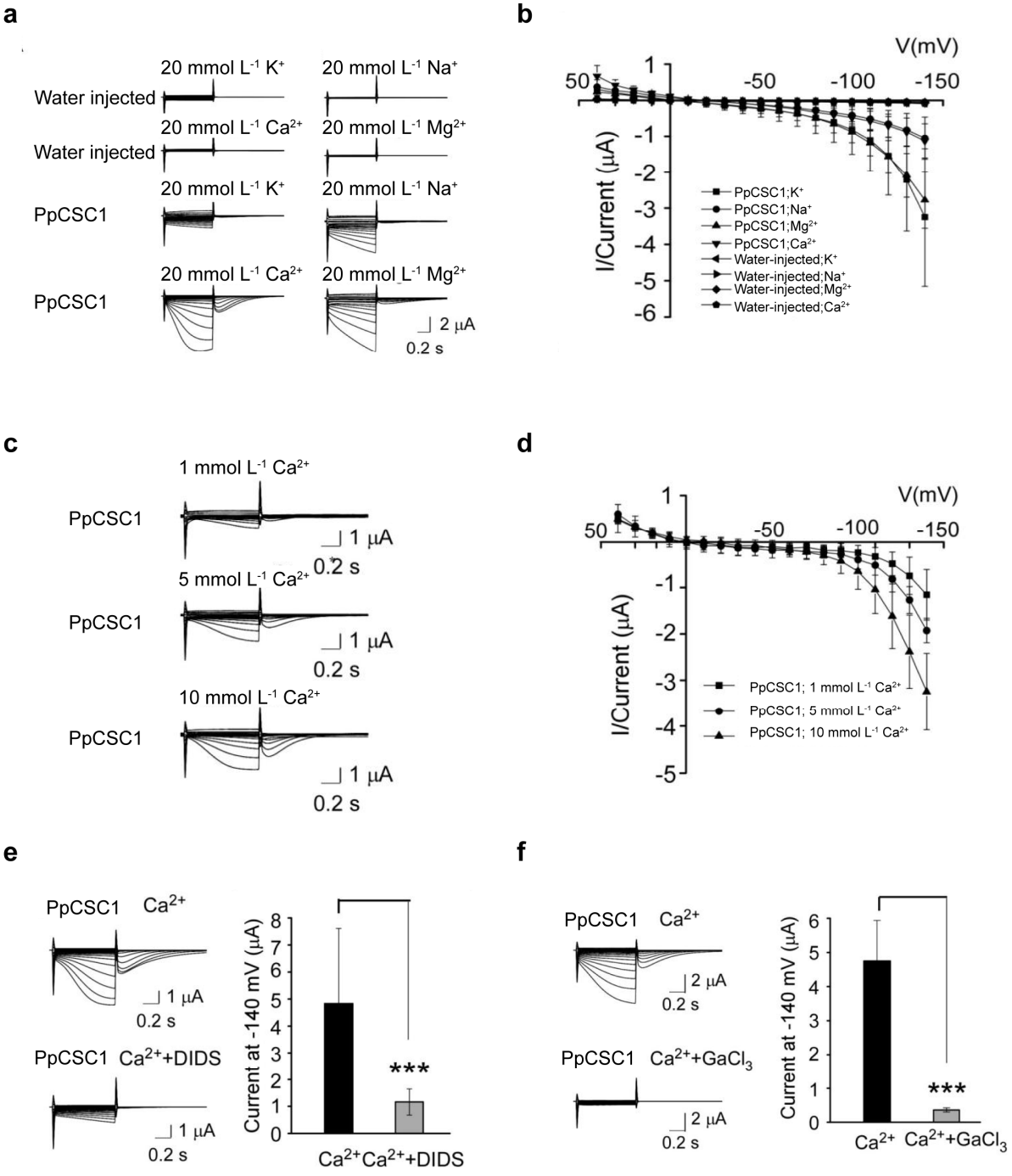

Figure 3: Electrophysiological characteristics of PpCSC1 in *Xenopus laevis* oocytes. (**a**, **b**) Representative whole-cell currents recorded from *Xenopus laevis* oocytes expressing *PpCSC1* in solutions containing 20 mmol L^{-1} K^+, Na^+, Ca^{2+}, or Mg^{2+}, with water-injected oocytes used as controls. (**c**, **d**) Electrophysiological signals recorded from *Xenopus laevi*

oocytes expressing PpCSC1, perfused with 1, 5 or 10 mmol L^{-1} Ca^{2+}. Water-injected oocytes served as controls. (**e**) Tail currents observed in PpCSC1-expressing *Xenopus laevis* oocytes in 20 mmol L^{-1} $CaCl_2$, with or without the Cl^- channel blocker DIDS. (**f**) Currents recorded from fifteen *PpCSC1*-expressing *Xenopus laevi* oocytes in 20 mmol L^{-1} $CaCl_2$ with or without $GaCl_3$ treatment. The current-voltage curves were plotted using GraphPad Prism. Values are shown as means ± SD of fifteen oocytes. Asterisks indicate significant difference between the conditions with and without inhibitor treatment, as determined by Student's *t*-test (***$p < 0.001$).

3.4 PpCSC1 Negatively Regulates Salt Tolerance in P. patens

To investigate the role of *PpCSC1* in abiotic stress tolerance, we first examined its transcriptional response to NaCl stress by qRT-PCR. In five-day-old protonemata, *PpCSC1* transcript levels progressively declined following NaCl treatment, reaching the lowest level at 8 h, and then partially recovered to one-third of the initial level at 24 h (Fig. 4a).

Further functional analysis was conducted by generating *PpCSC1*-overexpression (OE) lines, in which the coding sequence was placed under a strong promoter (Fig. 4b). After treatment with 350 mmol L^{-1} NaCl for 4 days, both wild-type (WT) and OE protonemata exhibited growth inhibition, whereas OE line with higher transcript levels exhibited more severe bleaching and browning (Fig. 4c), indicating reduced salt tolerance.

Ion content analysis revealed that, after 350 mmol L^{-1} NaCl treatment, K^+ levels were significantly lower in the OE line than in WT (Fig. 4d), while Na^+ content showed no significant difference (Fig. 4e). Consequently, the K^+/Na^+ ratio in the OE line was markedly decreased (Fig. 4f). The OE line also accumulated significantly more Mg^{2+} than the WT (Fig. 4g), while Ca^{2+} content remained unchanged (Fig. 4h).

Together, these results demonstrate that overexpression of *PpCSC1* disrupts ion homeostasis under salt stress, leading to K^+ loss and Mg^{2+} accumulation, which impairs salt tolerance.

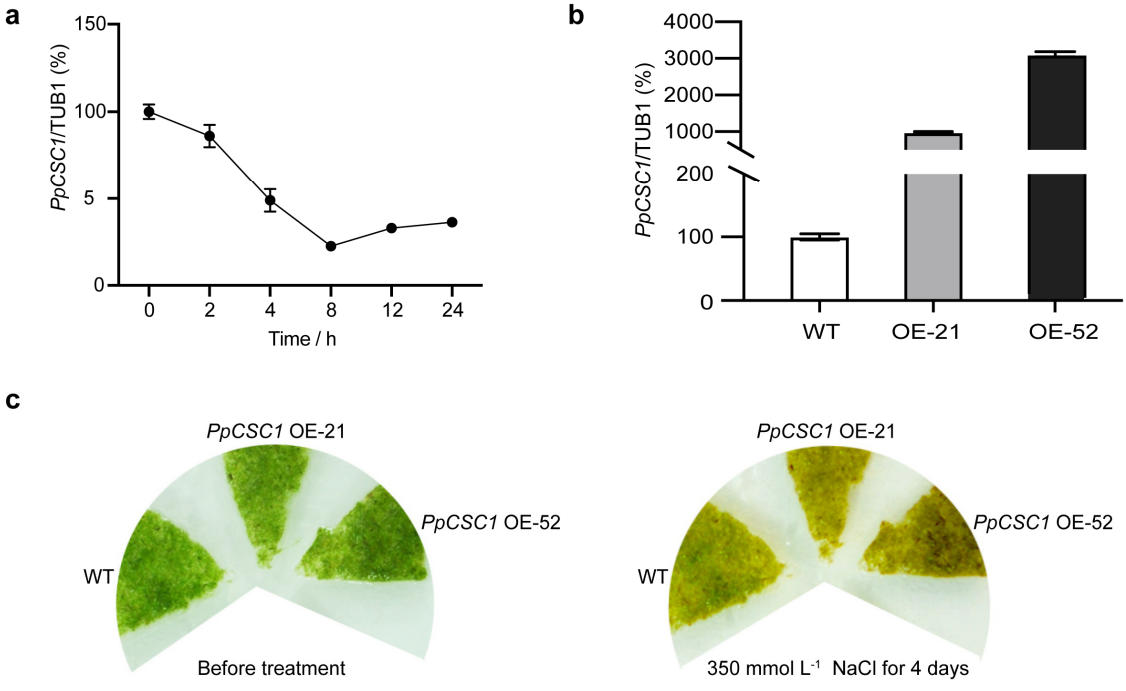

Figure 4: *Cont.*

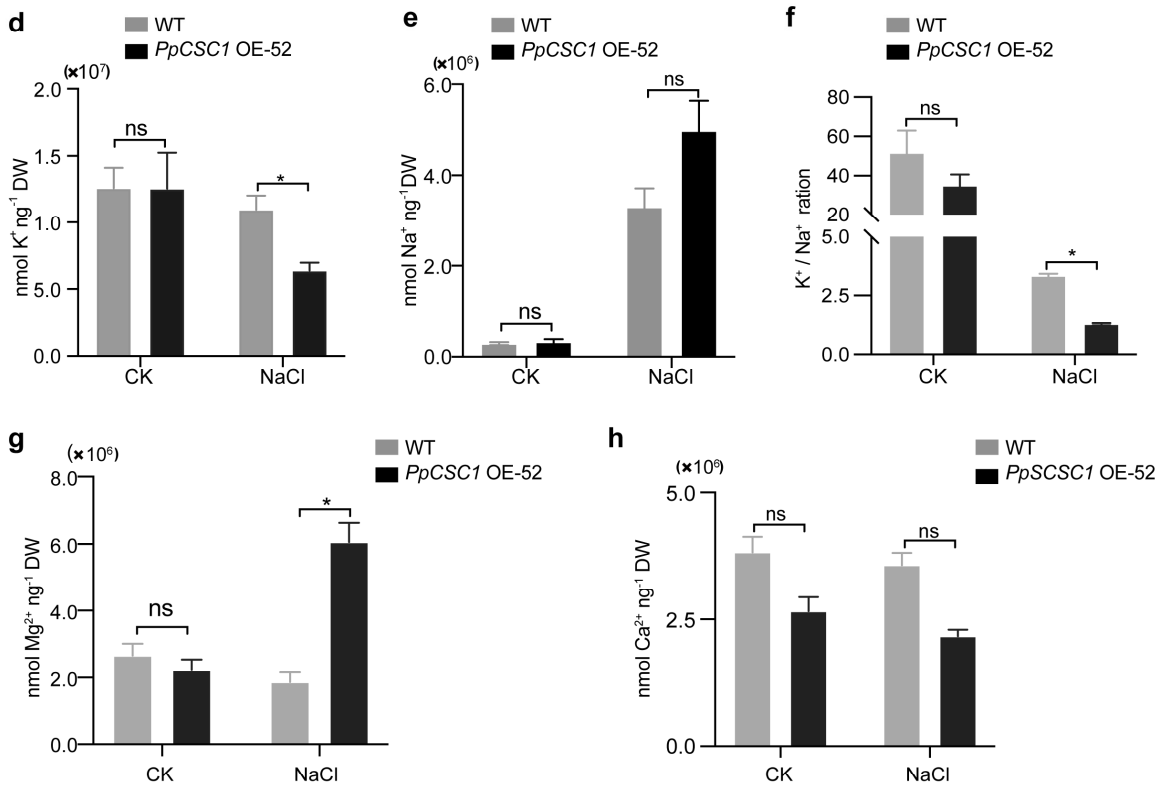

Figure 4: *PpCSC1* negatively regulates salt tolerance in *P. patens*. (**a**) Relative mRNA levels of *PpCSC1* after salt treatment. Five-day-old WT protonema were exposed to 350 mmol L^{-1} NaCl for 0, 2, 4, 8, 12, and 24 h. Transcript levels were normalized to *TUB1* as the internal control, with the expression level at 0 h set as the baseline (100%). Relative expression is presented as percentage values relative to the 0 h time point. Error bars represent the standard deviation of three biological replicates. (**b**) Transcription levels of *PpCSC1* in overexpression (OE) transgenic lines. Transcript levels were normalized to *TUB1*, with WT expression set as the baseline (100%). Relative expression is presented as percentage values relative to WT. Standard deviation was derived from three biological replicates. (**c**) Phenotypic analysis of *PpCSC1* OE plants under salt stress. Representative images show five-day-old protonemata before treatment and after 4 days of exposure to 350 mmol L^{-1} NaCl. (**d-h**) Cation contents in the *PpCSC1* OE plant under 350 mmol L^{-1} NaCl stress. After 3 days of NaCl treatment, K^+ content (**d**), Na^+ content (**e**), K^+/Na^+ contents (**f**), Mg^{2+} content (**g**) and Ca^{2+} content (**h**) were measured. Values are shown as means ± SD from three biological replicates. Asterisks indicate significant difference between WT and OE transgenic plant, as determined by Student's *t*-test (*$p < 0.05$). 'ns' indicates no significant difference.

3.5 PpCSC1 is Transcriptionally Regulated by PpSTOP2

We employed a gene interaction and co-expression network centered on *PpCSC1* to identify its upstream regulators. This approach identified a C2H2-type zinc finger transcription factor PpSTOP2 as a strong regulatory candidate. Phylogenetic and sequence analyses revealed that PpSTOP2 is a 609-amino acid protein and the moss homolog of PpSTOP1 (Fig. 5a,b).

The regulatory influence of PpSTOP2 on *PpCSC1* was examined using dual-luciferase (LUC) reporter assays in *A. thaliana* protoplasts. Effector constructs containing progressive deletions of the *PpCSC1* promoter (−534, −1334, and −1984 bp upstream of the transcription start site) were co-transformed with a *35S::PpSTOP2* reporter plasmid. The strongest induction of LUC activity occurred only when the −1334 to −1984 bp promoter region was present (Fig. 5c). Chromatin immunoprecipitation (ChIP-qPCR) further

confirmed that PpSTOP2 is specifically enriched at the −1334 to −1984 bp region of the *PpCSC1* promoter (Fig. 5d). Together, these results indicate that PpSTOP2 regulates *PpCSC1* transcription by directly binding to the −1334 to −1984 bp promoter fragment.

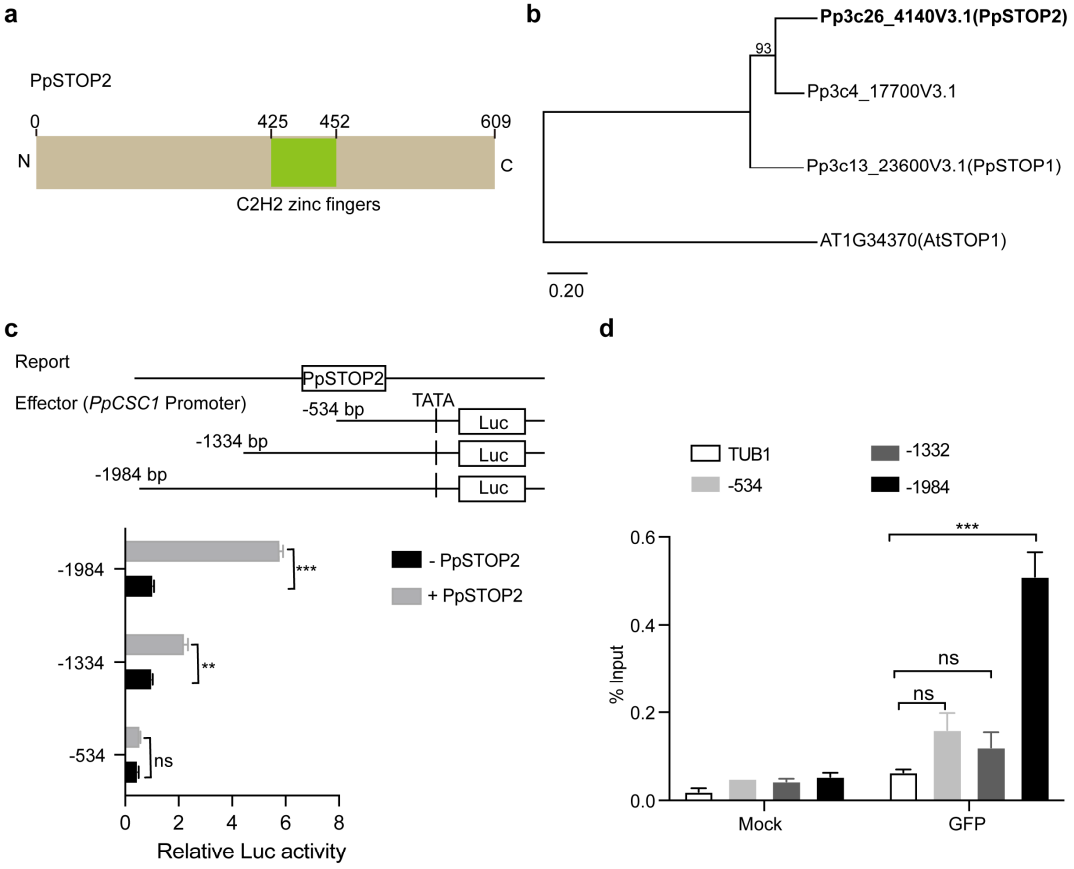

Figure 5: Regulation of *PpCSC1* by the transcription factor PpSTOP2. (**a**) Predicted domain architecture of PpSTOP2. The positions of the C2H2 zinc finger motifs are indicated. (**b**) Phylogenetic tree of PpSTOP orthologs in *P. patens*. Maximum-likelihood analysis was performed using the PpSTOP1 family. Bootstrap support values (1000 replicates) are shown next to branches, and the scale bar represents the number of substitutions per site. (**c**) Transcriptional activation assay of *PpCSC1* by PpSTOP2. A schematic of the *pPpCSC1::LUC* reporter and PpSTOP2 effectors (top). The *PpCSC1* promoter was divided into three fragments: −1 to −1984 bp (−1984), −1 to −1334 bp (−1334), and −1 to −534 bp (−534). LUC activity was used to evaluate transcriptional activation, with GUS as a control. (**d**) ChIP-qPCR validation of PpSTOP2 binding to the *PpCSC1* promoter. Promoter structure and corresponding amplified fragments analyzed are shown in (**c**). ChIP assays were performed using anti-GFP antibody, with GFP as the antibody control and the *PpTubulin* promoter (TuB1) as a negative control. The values are shown as means ± SD of three repeats. Asterisks indicate significant difference between wild-type and other genetic materials, as determined by Student's *t*-test (**$p < 0.01$, ***$p < 0.001$). 'ns' indicates no significant difference.

3.6 PpSTOP2 Negatively Influences Salt Tolerance

The expression dynamics of *PpSTOP2* under NaCl stress were analyzed by qRT-PCR. In five-day-old protonemata, *PpSTOP2* expression was transiently induced at 2–4 h and subsequently declined (Fig. 6a).

Further functional characterization was carried out by generating *PpSTOP2* knockout (KO) mutants using CRISPR/Cas9 (Fig. 6b). After 4 days of exposure to 500 mmol L^{-1} NaCl, wild-type protonemata

displayed severe bleaching, whereas *PpSTOP2* KO lines retained green tissue and continued to grow (Fig. 6c). Consistent with this phenotype, chlorophyll content remained significantly higher in *PpSTOP2* KO lines under salt stress (Fig. 6d), indicating that loss of *PpSTOP2* enhances salt tolerance. Given this phenotype, we next examined whether PpSTOP2 regulates *PpCSC1* transcription *in vivo*. qRT-PCR analysis revealed that *PpCSC1* transcript levels were consistently lower in *PpSTOP2* KO than in WT protonemata at 12 and 24 h after NaCl treatment (Fig. 6e). Together, these results suggest that PpSTOP2 positively regulates *PpCSC1* expression, thereby compromising salt tolerance in *P. patens*.

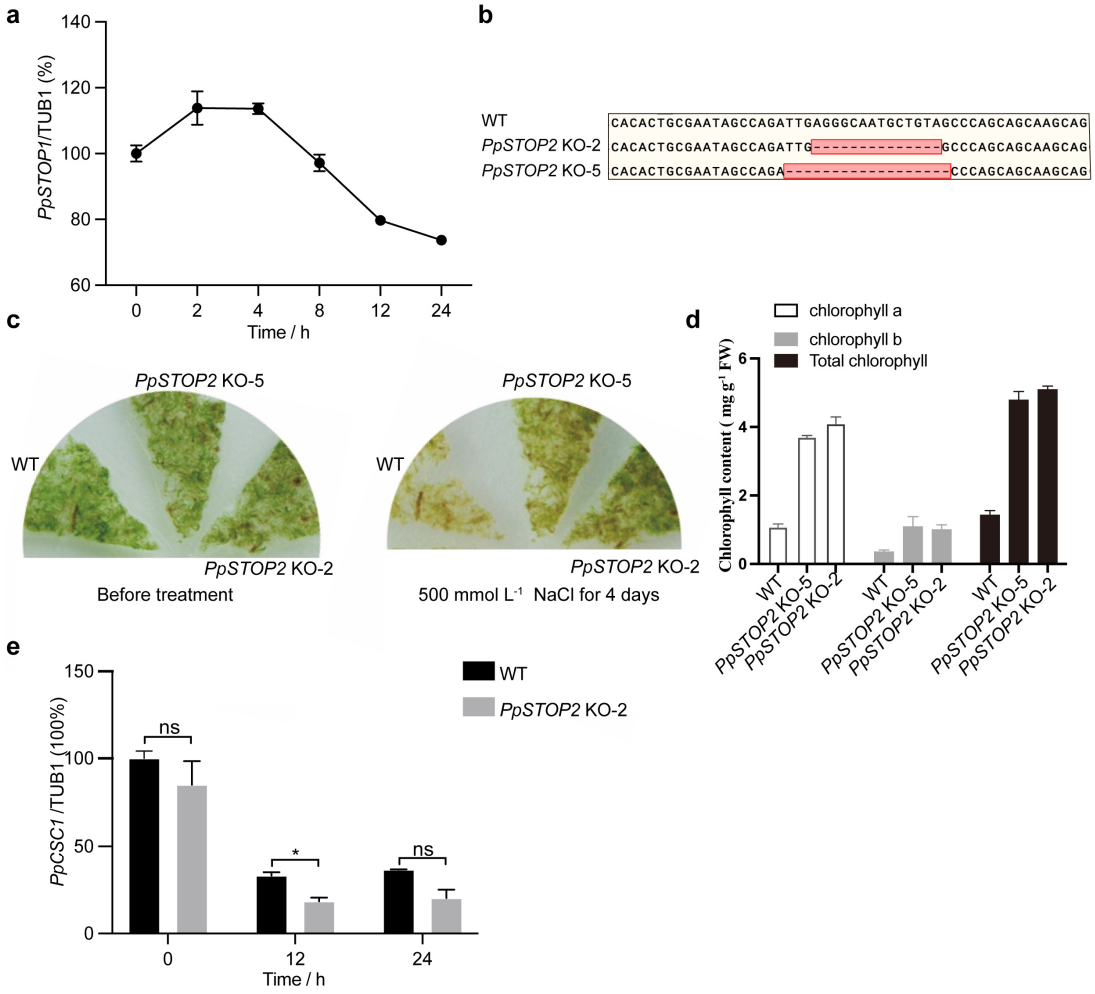

Figure 6: *PpSTOP2* negatively regulates salt resistance in *P. patens*. (**a**) Relative mRNA levels of *PpSTOP2* after salt treatment. Five-day-old WT protonema were subjected to 350 mmol L^{-1} NaCl treatment for 0, 2, 4, 8, 12, and 24 h respectively. (**b**) Partial genomic sequences of WT and *PpSTOP2* alleles. (**c**) Representative photograph of *PpSTOP2* KO and WT plants on BCD media with 500 mmol L^{-1} NaCl for 4 days. (**d**) Total chlorophyll contents of WT and *PpSTOP2* KO protonema after 500 mmol L^{-1} NaCl treatment for 4 days (**e**) Relative mRNA levels of *PpCSC1*. Five-day-old WT protonema and *PpSTOP2* KO-2 were treated with 500 mmol L^{-1} NaCl treatment. Transcript levels were normalized to *TUB1* as the internal control, with the expression level at 0 h set as the baseline (100%). Relative expression was presented as percentage values relative to the 0-h time point. Error bars represent the standard deviation of three biological replicates. The values are shown as means ± SD of three repeats. Asterisks indicate significant difference between wild-type and other genetic materials, as determined by Student's *t*-test (*$p < 0.05$). 'ns' indicates no significant difference.

4 Discussion

Phylogenetic analysis revealed that bryophyte ERD4 homologs form distinct subclades within the OSCA/AtCSC family, separate from angiosperm homologs (Fig. 1b). This divergence likely predates the emergence of vascular plants, indicating that ERD4 diversification occurred early in land plant evolution. Despite this evolutionary separation, bryophyte ERD4 homologs, including PpCSC1, retain the conserved DUF221 domain characteristic of the ERD4 family, supporting their structural homology with OSCA proteins in vascular plants. The presence of multiple ERD4 homologs in *P. patens* further suggests potential functional redundancy, which may obscure phenotypes in single-gene knockout lines. Therefore, comprehensive analyses that integrate expression profiling, subcellular localization, and ion selectivity will be necessary to elucidate the distinct functions of each family member.

Functionally, our electrophysiological and physiological analyses demonstrate that PpCSC1 acts as a non-selective cation channel permeable to Na^+, K^+, Ca^{2+}, and Mg^{2+}. Unlike vascular plant OSCAs, which positively contribute to stress adaptation by initiating Ca^{2+} signaling [16,17,62]. *PpCSC1* functions as a negative regulator of salt tolerance (Fig. 4). Overexpression of *PpCSC1* decreases the K^+/Na^+ ratio, perturbs ionic balance, and inhibits growth under salinity stress, implying that channel activity must be tightly constrained in moss to avoid maladaptive ion fluxes. This distinct physiological role emphasizes the expanded diversity of ion selectivity within ERD4 family: whereas vascular homologs predominantly link osmotic perception to Ca^{2+}-based signaling, *PpCSC1* primarily modulates bulk cation fluxes, highlighting functional diversification of ERD4 proteins in land plants.

In *Arabidopsis thaliana*, ERD4 homologs such as OSCA1, OSCA3.1, and AtCSC1 act as mechanosensitive channels whose activation depends on membrane tension or osmotic fluctuations [16,17,62]. By contrast, overexpression of *PpCSC1* in *Xenopus laevis* oocytes produces substantial basal currents in the absence of mechanical stimulation, suggesting that the channel has an intrinsic ion-conducting capacity. This phenomenon is more likely a consequence of protein overexpression in the heterologous system rather than a reflection of its physiological behavior, and thus does not exclude the mechanosensitive nature of PpCSC1. In its native *P. patens* cellular context, activation of PpCSC1 is more likely to depend on mechanical signals, such as osmotic stress or membrane stretching, with its precise regulatory mechanisms remaining to be elucidated. Moreover, the lipid composition of the moss plasma membrane and potential interacting proteins may be critical for constraining or fine-tuning channel activity. Taken together, these findings indicate that while ERD4 channels are conserved in ion selectivity and mechanosensitivity, their regulatory modes have diversified among plant lineages, reflecting evolutionary adaptation to distinct cellular and ecological contexts.

This physiological gating constraint is complemented by transcriptional regulation through PpSTOP2. PpSTOP2 activates *PpCSC1* expression and displays biphasic dynamics under salt stress: rapid induction during the early phase, followed by strong repression (Fig. 6a). This feedback ensures transient channel activation for signaling while preventing prolonged cation influx and associated ionic toxicity. By contrast, in angiosperms such as *A. thaliana* and *O. sativa*, STOP1-like factors (AtSTOP1, OsART1) exhibit stable expression and protein activity under acid or aluminum stress, sustaining downstream transporter activation (e.g., *ALMT1*, *MATE*, *ALS3*) to promote detoxification [24,27,45,51]. Thus, whereas vascular plants rely on transcriptional activation of transporter pathways, mosses employ a dual-layered regulatory system-mechanosensitive gating at the protein level and biphasic transcriptional control at the gene level-to fine-tune channel activity (Fig. 7).

Collectively, these findings highlight a fundamental divergence in stress adaptation strategies between bryophytes and vascular plants. Bryophytes achieve tolerance primarily by restricting channel activity to

maintain ionic homeostasis, whereas vascular plants enhance tolerance by sustaining activation through stable transcriptional programs. This divergence likely reflects fundamental differences in vacuolar capacity, tissue complexity, and ion compartmentalization between early and advanced land plants. The discovery of the PpSTOP2-PpCSC1 regulatory module not only broadens the functional landscape of ERD4 protein but also underscores the evolutionary plasticity of transcriptional and post-translational control in stress signaling. Future studies should determine whether other moss ERD4 paralogs act redundantly or divergently in abiotic stress responses, and how their functions integrate with Ca^{2+}-based signaling pathways typical of vascular ERD4 protein.

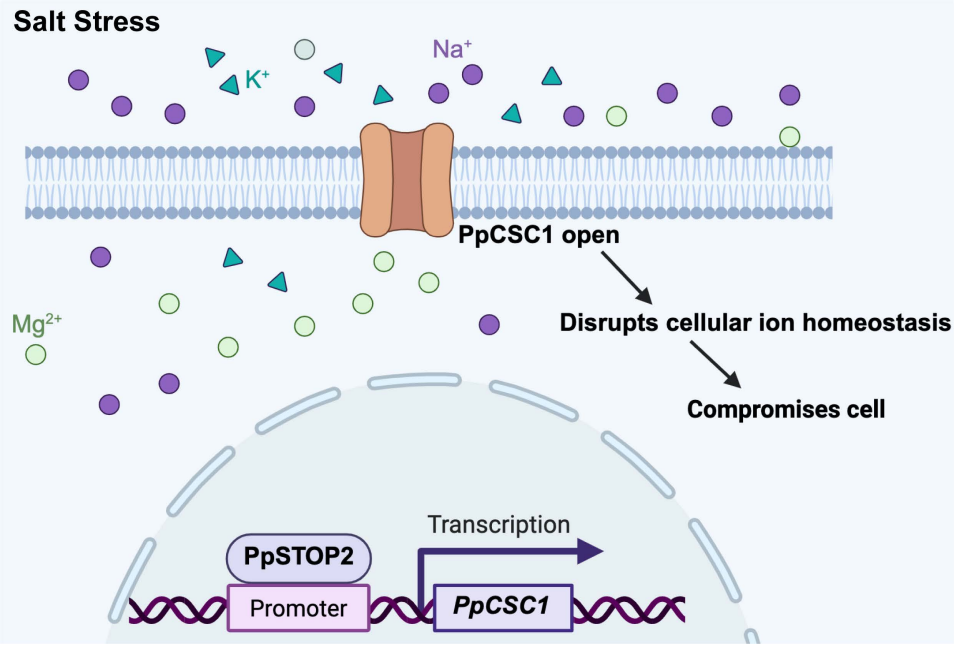

Figure 7: Model of the PpSTOP2-PpCSC1 regulatory module under salt stress. Under salt stress, the transcription factor PpSTOP2 binds to the promoter of *PpCSC1* and activates its transcription. The resulting PpCSC1 protein localizes to the plasma membrane and functions as a non-selective cation channel permeable to Na^+, K^+, Mg^{2+}, and Ca^{2+}. When PpCSC1 channels open, excessive cation flux reduces the K^+/Na^+ ratio, disrupts cellular ion homeostasis, and ultimately impaires cellular function and reduced stress tolerance.

Acknowledgement: Fig. 7 was created with BioRender.com.

Funding Statement: This work was supported by the National Natural Science Foundation of China (Grant No. 31970658 and No. 32400208), the Zhejiang Provincial Natural Science Foundation of China (Grant No. LD24C130002 and No. LQN25C020001), and the Scientific Research Foundation of China Jiliang University.

Author Contributions: The authors confirm contributions to the paper as follows: Fang Bao, Yikun He, and Lu Chen conceived and designed the research and wrote the manuscript. Sheng Teng provided critical analyses and revised the manuscript. Lu Chen performed most of the experiments and contributed to manuscript editing. Legong Li and Zhijie Ren carried out the voltage-clamp experiments. Guangmin Zhao performed the ChIP-qPCR assays. Xuan He optimized the CRISPR/Cas9 system for *PpSTOP2* knockout in *Physcomitrium patens*. All authors reviewed the results and approved the final version of the manuscript.

Availability of Data and Materials: Not applicable.

Ethics Approval: Not applicable.

Conflicts of Interest: The authors declare no conflicts of interest to report regarding the present study.

References

1. Ma L, Liu X, Lv W, Yang Y. Molecular mechanisms of plant responses to salt stress. Front Plant Sci. 2022;13:934877. [CrossRef].
2. Zhao S, Zhang Q, Liu M, Zhou H, Ma C, Wang P. Regulation of plant responses to salt stress. Int J Mol Sci. 2021;22(9):4609. [CrossRef].
3. Slama I, Abdelly C, Bouchereau A, Flowers T, Savoure A. Diversity, distribution and roles of osmoprotective compounds accumulated in halophytes under abiotic stress. Ann Bot. 2015;115(3):433–47. [CrossRef].
4. Munns R, Tester M. Mechanisms of salinity tolerance. Annu Rev Plant Biol. 2008;59:651–81. [CrossRef].
5. Zhou H, Shi H, Yang Y, Feng X, Chen X, Xiao F, et al. Insights into plant salt stress signaling and tolerance. J Genet Genomics. 2024;51(1):16–34. [CrossRef].
6. Yu Z, Duan X, Luo L, Dai S, Ding Z, Xia G. How plant hormones mediate salt stress responses. Trends Plant Sci. 2020;25(11):1117–30. [CrossRef].
7. Zhu JK. Abiotic stress signaling and responses in plants. Cell Rep. 2016;167:313–24. [CrossRef].
8. Zhu JK. Salt and drought stress signal transduction in plants. Annu Rev Plant Biol. 2002;53:247–73. [CrossRef].
9. Joshi S, Nath J, Singh AK, Pareek A, Joshi R. Ion transporters and their regulatory signal transduction mechanisms for salinity tolerance in plants. Physiol Plant. 2022;174(3):e13702. [CrossRef].
10. Zuo Y, Abbas A, Dauda SO, Chen C, Bose J, Donovan-Mak M, et al. Function of key ion channels in abiotic stresses and stomatal dynamics. Plant Physiol Biochem. 2025;220:109574. [CrossRef].
11. Liu L, Li X, Wang C, Ni Y, Liu X. The role of chloride channels in plant responses to NaCl. Int J Mol Sci. 2023;25(1):19. [CrossRef].
12. Mostofa MG, Rahman MM, Ghosh TK, Kabir AH, Abdelrahman M, Rahman Khan MA, et al. Potassium in plant physiological adaptation to abiotic stresses. Plant Physiol Biochem. 2022;186:279–89. [CrossRef].
13. Amin I, Rasool S, Mir MA, Wani W, Masoodi KZ, Ahmad P. Ion homeostasis for salinity tolerance in plants: a molecular approach. Physiol Plant. 2021;171(4):578–94. [CrossRef].
14. Taji T, Seki M, Yamaguchi-Shinozaki K, Kamada H, Giraudat J, Shinozaki K. Mapping of 25 drought-inducible genes, RD and ERD, in *Arabidopsis thaliana*. Plant Cell Physiol. 1999;40(1):119–23. [CrossRef].
15. Kiyosue T, Yamaguchi-Shinozaki K, Shinozaki K. Cloning of cDNAs for genes that are early-responsive to dehydration stress (ERDs) in *Arabidopsis thaliana* L.: identification of three ERDs as HSP cognate genes. Plant Mol Biol. 1994;25(5):791–8. [CrossRef].
16. Yuan F, Yang H, Xue Y, Kong D, Ye R, Li CJ, et al. OSCA1 mediates osmotic-stress-evoked Ca^{2+} increases vital for osmosensing in Arabidopsis. Nature. 2014;514(7522):367–71. [CrossRef].
17. Hou C, Tian W, Kleist T, He K, Garcia V, Bai F, et al. DUF221 proteins are a family of osmosensitive calcium-permeable cation channels conserved across eukaryotes. Cell Res. 2014;24:632–5. [CrossRef].
18. Rai A, Suprasanna P, D'Souza SF, Kumar V. Membrane topology and predicted RNA-binding function of the 'early responsive to dehydration (ERD4)' plant protein. PLoS One. 2012;7(3):e32658. [CrossRef].
19. Jaroszewski L, Li Z, Krishna SS, Bakolitsa C, Wooley J, Deacon AM, et al. Exploration of uncharted regions of the protein universe. PLoS Biol. 2009;7:e1000205. [CrossRef].
20. Shan Y, Zhang M, Chen M, Guo X, Li Y, Zhang M, et al. Activation mechanisms of dimeric mechanosensitive OSCA/TMEM63 channels. Nat Commun. 2024;15(1):7504. [CrossRef].
21. Han Y, Zhou Z, Jin R, Dai F, Ge Y, Ju XS, et al. Mechanical activation opens a lipid-lined pore in OSCA ion channels. Nature. 2024;628(8009):910–8. [CrossRef].
22. Zhang M, Wang D, Kang Y, Wu JX, Yao F, Pan CF, et al. Structure of the mechanosensitive OSCA channels. Nat Struct Mol Biol. 2018;25(9):850–8. [CrossRef].
23. Zhang M, Shan Y, Cox CD, Pei D. A mechanical-coupling mechanism in OSCA/TMEM63 channel mechanosensitivity. Nat Commun. 2023;14(1):3943. [CrossRef].
24. Liu Y, Li H, Shi Y, Song Y, Wang T, Li Y. A maize early responsive to dehydration gene, ZmERD4, provides enhanced drought and salt tolerance in arabidopsis. Plant Mol Biol Report. 2009;27(4):542–8. [CrossRef].

25. Rensing SA, Goffinet B, Meyberg R, Wu SZ, Bezanilla M. The Moss *Physcomitrium (Physcomitrella) patens*: a model organism for non-seed plants. Plant Cell. 2020;32(5):1361–76. [CrossRef].
26. Wang XQ, Yang PF, Liu Z, Liu WZ, Hu Y, Chen H, et al. Exploring the mechanism of *Physcomitrella patens* desiccation tolerance through a proteomic strategy. Plant Physiol. 2009;149(4):1739–50. [CrossRef].
27. Saavedra L, Svensson J, Carballo V, Izmendi D, Welin B, Vidal S. A dehydrin gene in *Physcomitrella patens* is required for salt and osmotic stress tolerance. Plant J. 2006;45:237–49. [CrossRef].
28. Frank W, Ratnadewi D, Reski R. *Physcomitrella patens* is highly tolerant against drought, salt and osmotic stress. Planta. 2005;220(3):384–94. [CrossRef].
29. Haro R, Fraile-Escanciano A, González-Melendi P, Rodríguez-Navarro A. The potassium transporters HAK2 and HAK3 localize to endomembranes in Physcomitrella patens. HAK2 is required in some stress conditions. Plant Cell Physiol. 2013;54(9):1441–54. [CrossRef].
30. Oh DH, Ali A, Yun DJ, Bressan RA, Jin JB. SOS1 and AtHKT1;1 transporters mediate long-distance Na^+ transport in Arabidopsis. Plant Signal Behav. 2010;5(8):1034–6. [CrossRef].
31. Fraile-Escanciano A, Kamisugi Y, Cuming AC, Rodríguez-Navarro A, Benito B. The SOS1 transporter of *Physcomitrella patens* mediates sodium efflux in planta. New Phytol. 2010;188(3):750–61. [CrossRef].
32. Fraile-Escanciano A, Garciadeblás B, Rodríguez-Navarro A, Benito B. Role of ENA ATPase in Na^+ efflux at high pH in bryophytes. Plant Mol Biol. 2009;71(6):599–608. [CrossRef].
33. Barrero-Gil J, Rodríguez-Navarro A, Benito B. Cloning of the PpNHAD1 transporter of Physcomitrella patens, a chloroplast transporter highly conserved in photosynthetic eukaryotic organisms. J Exp Bot. 2007;58(11):2839–49. [CrossRef].
34. Koochak H, Ludwig-Muller J. *Physcomitrium patens* mutants in auxin conjugating GH3 proteins show salt stress tolerance but auxin homeostasis is not involved in regulation of oxidative stress factors. Plants. 2021;10(7):1398. [CrossRef].
35. Chen L, Bao F, Tang S, Zuo E, Lv Q, Zhang DY, et al. PpAKR1A, a novel Aldo-Keto reductase from *Physcomitrella Patens*, plays a positive role in salt stress. Int J Mol Sci. 2019;20(22):5723. [CrossRef].
36. Xiao F, Li XC, He JX, Zhao JF, Wu GC, Gong QY, et al. Protein kinase PpCIPK1 modulates plant salt tolerance in *Physcomitrella patens*. Plant Mol Biol. 2021;105(6):685–96. [CrossRef].
37. Hyoung SJ, Cho SH, Chung JH, So WM, Cui MH, Shin JS. Cytokinin oxidase PpCKX1 plays regulatory roles in development and enhances dehydration and salt tolerance in *Physcomitrella patens*. Plant Cell Rep. 2020;39(3):419–30. [CrossRef].
38. Do TH, Pongthai P, Ariyarathne M, Teh OK, Fujita T. AP2/ERF transcription factors regulate salt-induced chloroplast division in the moss *Physcomitrella patens*. J Plant Res. 2020;133(4):537–48. [CrossRef].
39. Li P, Yang H, Liu GJ, Ma WZ, Li CH, Huo HQ, et al. PpSARK regulates moss senescence and salt tolerance through ABA related pathway. Int J Mol Sci. 2018;19(9):2609. [CrossRef].
40. Du J, Wang L, Zhang XC, Xiao X, Wang F, Lin PL, et al. Heterologous expression of two *Physcomitrella patens* group 3 late embryogenesis abundant protein (LEA3) genes confers salinity tolerance in arabidopsis. J Plant Biol. 2016;59(2):182–93. [CrossRef].
41. Saavedra L, Balbi V, Dove SK, Hiwatashi YJ, Mikami K, Marianne Sommarin M. Characterization of phosphatidylinositol phosphate kinases from the moss *Physcomitrella patens*: PpPIPK1 and PpPIPK2. Plant Cell Physiol. 2009;50(3):595–609. [CrossRef].
42. Sadhukhan A, Kobayashi Y, Iuchi S, Koyama H. Synergistic and antagonistic pleiotropy of STOP1 in stress tolerance. Trends Plant Sci. 2021;26(10):1014–22. [CrossRef].
43. Huang CF, Ma Y. Aluminum resistance in plants: a critical review focusing on STOP1. Plant Commun. 2025;6(2):101200. [CrossRef].
44. Li X, Tian Y. STOP1 and STOP1-like proteins, key transcription factors to cope with acid soil syndrome. Front Plant Sci. 2023;14:1200139. [CrossRef].
45. Fan N, Li XB, Xie WX, Wei X, Fang Q, Huang CF. Modulation of external and internal aluminum resistance by ALS3-dependent STAR1-mediated promotion of STOP1 degradation. New Phytol. 2024;244(2):511–27. [CrossRef].
46. Silva-Navas J, Salvador N, Del Pozo JC, Benito C, Gallego FJ. The rye transcription factor ScSTOP1 regulates the tolerance to aluminum by activating the ALMT1 transporter. Plant Sci. 2021;310:110951. [CrossRef].

47. Sawaki Y, Iuchi S, Kobayashi Y, Kobayashi Y, Ikka T, Sakurai N, et al. STOP1 regulates multiple genes that protect arabidopsis from proton and aluminum toxicities. Plant Physiol. 2009;150(1):281–94. [CrossRef].
48. Liu J, Magalhaes JV, Shaff J, Kochian LV. Aluminum-activated citrate and malate transporters from the MATE and ALMT families function independently to confer Arabidopsis aluminum tolerance. Plant J. 2009;57(3):389–99. [CrossRef].
49. Huang S, Gao J, You J, Liang Y, Guan K, Yan SQ, et al. Identification of STOP1-like proteins associated with aluminum tolerance in sweet sorghum (*Sorghum bicolor* L.). Front Plant Sci. 2018;9:258. [CrossRef].
50. Che J, Tsutsui T, Yokosho K, Yamaji N, Ma JF. Functional characterization of an aluminum (Al)-inducible transcription factor, ART2, revealed a different pathway for Al tolerance in rice. New Phytol. 2018;220(1):209–18. [CrossRef].
51. Yamaji N, Huang CF, Nagao S, Yano M, Sato Y, Nagamura Y, et al. A zinc finger transcription factor ART1 regulates multiple genes implicated in aluminum tolerance in rice. Plant Cell. 2009;21(10):3339–49. [CrossRef].
52. Magalhaes JV, Liu J, Guimaraes CT, Lana UG, Alves VM, Wang YH, et al. A gene in the multidrug and toxic compound extrusion (MATE) family confers aluminum tolerance in sorghum. Nat Genet. 2007;39(9):1156–61. [CrossRef].
53. Furukawa J, Yamaji N, Wang H, Mitani N, Murata Y, Sato K, et al. An aluminum-activated citrate transporter in barley. Plant Cell Physiol. 2007;48(8):1081–91. [CrossRef].
54. Ćosić MV, Božović DP, Jadranin B, Vujičić MM, Sabovljević AD, Sabovljević MS. Axenic cultivation of bryophytes: growth media composition. Plant Cell Tissue Organ Cult. 2025;160(2):276217461. [CrossRef].
55. Wang X, Zhou S, Chen L, Quatrano RS, He YK. Phospho-proteomic analysis of developmental reprogramming in the moss *Physcomitrella patens*. J Proteomics. 2014;108:284–94. [CrossRef].
56. Cove DJ, Perroud PF, Charron AJ, McDaniel SF, Khandelwal A, Quatrano RS. The moss *Physcomitrella patens*: a novel model system for plant development and genomic studies. Cold Spring Harb Protoc. 2009;2009:115. [CrossRef].
57. Wu GC, Li S, Li XC, Liu YH, Zhao SS, Liu BH, et al. A Functional Alternative Oxidase Modulates Plant Salt Tolerance in *Physcomitrella patens*. Plant Cell Physiol. 2019;60(8):1829–41. [CrossRef].
58. Rao XY, Huang XL, Zhou ZC, Lin X. An improvement of the $2^{-\Delta\Delta Ct}$ method for quantitative real-time polymerase chain reaction data analysis. Biostat Bioinforma Biomath. 2013;3(3):71–85.
59. Livak KJ, Schmittgen TD. Analysis of relative gene expression data using real-time quantitative PCR and the $2^{-\Delta\Delta Ct}$ method. Methods. 2001;25(4):402–8. [CrossRef].
60. Lopez-Obando M, Hoffmann H, Géry C, Guyon-Debast A, Téoulé E, Rameau C, et al. G3 genes genom. Simple and Efficient targeting of multiple genes through CRISPR-Cas9 in *Physcomitrella patens*. Genetica. 2016;6:3647–53. [CrossRef].
61. Abel S, Theologis A. Transient transformation of Arabidopsis leaf protoplasts: a versatile experimental system to study gene expression. Plant J. 1994;5(3):421–7. [CrossRef].
62. Pei S, Tao Q, Li W, Qi G, Wang B, Wang Y, et al. Osmosensor-mediated control of Ca^{2+} spiking in pollen germination. Nature. 2024;629:1118–25. [CrossRef].